Microscopic analysis of electron noise in GaAs Schottky barrier diodes

Tomás González[a] and Daniel Pardo
Departamento de Física Aplicada, Facultad de Ciencias, Universidad de Salamanca, Plaza de la Merced s/n, 37008 Salamanca, Spain

Lino Reggiani
Istituto Nazionale di Fisica della Materia, Dipartimento di Scienza dei Materiali, Università di Lecce, Via Arnesano, 73100 Lecce, Italy

Luca Varani
Centre d'Electronique et de Micro-Optoelectronique de Montpellier (CNRS UMR 5507), Université Montpellier II, F-34095 Montpellier Cedex 5, France

(Received 7 February 1997; accepted for publication 23 May 1997)

A microscopic analysis of current and voltage fluctuations in GaAs Schottky barrier diodes under forward-bias conditions in the absence of $1/f$ contributions is presented. Calculations are performed by coupling self-consistently an ensemble Monte Carlo simulator with a one-dimensional Poisson solver. By using current- and voltage-operation modes the microscopic origin and the spatial location of the noise sources, respectively, is provided. At different voltages the device exhibits different types of noise (shot, thermal, and excess), which are explained as a result of the coupling between fluctuations in carrier velocity and self-consistent field. The essential role of the field fluctuations to correctly determine the noise properties in these diodes is demonstrated. The results obtained for the equivalent noise temperature are found to reproduce the typical behavior of experimental measurements. An equivalent circuit is proposed to predict and explain the noise spectra of the device under thermionic emission-based operation. © *1997 American Institute of Physics.* [S0021-8979(97)01817-3]

I. INTRODUCTION

The excellent high-frequency behavior of Schottky barrier diodes (SBDs) is at the origin of their increasing employment for several applications, such as mixers and detectors of signals up to frequencies of some hundred gigahertz and even terahertz,[1] as in the case of heterodyne receivers.[2] The current-voltage characteristics of these devices have been extensively treated in the literature,[3–6] and several numerical models for their simulation have been developed.[7–13] Among these some Monte Carlo (MC) simulations under forward-bias conditions have also been successfully performed.[8,11–13] However, the quality factor of the SBD applications at these very high frequencies is limited by their noise.[14] Hence, in addition to static characteristics, a detailed characterization of the noise performance in these devices is a mandatory issue. On this ground, the noise temperature is one of the most important parameters to be determined. In recent years this subject has received special attention.[15–18] However, the use of phenomenological approaches makes an unambiguous identification of the noise sources difficult. Therefore, a microscopic interpretation of the processes causing the noise remains a major objective. By providing an exact solution of the appropriate kinetic equation, the MC technique, which has already been proven to be a powerful tool for the noise analysis of semiconductor devices,[19] is especially appropriate to this scope.[20–22] In the present work we employ an ensemble MC simulator coupled with a one-dimensional Poisson solver (PS). The application of this method avoids any *ad hoc* assumption and/or simplification about the properties of the noise sources, and thus gives a unifying microscopic analysis of the processes responsible for the fluctuations.

The purpose of this article is to present the results of a theoretical study of the noise characteristics (both of current and voltage) of GaAs SBDs under forward-bias conditions, thus completing and extending preliminary reports on the subject.[20,21] We aim at providing a comprehensive interpretation of the noise spectra in these devices in terms of the microscopic processes responsible of the fluctuations. By intrinsically incorporating the details of the noise sources and including the self-consistent field fluctuations, the MC technique used in this work offers a reliable test for the physical interpretation of noise performances in SBDs. The typical transport regimes of SBDs, that is, thermionic emission, series resistance, and hot carrier conditions, and the corresponding noise performances, are naturally reproduced with our approach. In particular, we will prove the essential role of the field fluctuations to correctly determine the noise properties in these devices.

The paper is organized as follows: Section II describes the physical model used to simulate the SBD. In Sec. III we present the theoretical basis of the operation modes under which the noise in the diodes is analyzed. Section IV is devoted to the presentation and discussion of the results concerning static characteristics, current noise, voltage noise, noise temperature and small-signal equivalent circuit. Major conclusions are summarized in Sec. V.

II. PHYSICAL MODEL

Most of the results of this work correspond to a SBD modeled as a one-dimensional GaAs n^+-n-metal structure as

[a]Electronic mail:tomasg@rs6000.usal.es

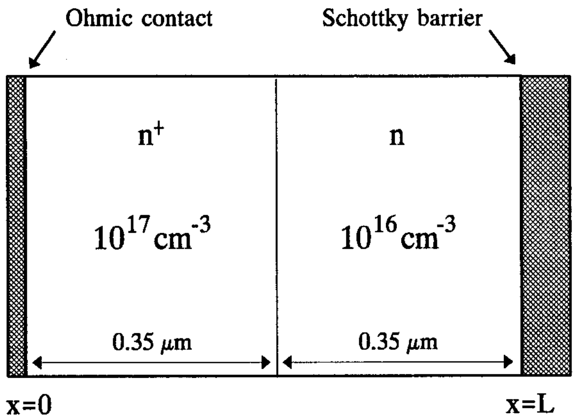

FIG. 1. Schematic drawing of the Schottky barrier diode under study.

shown schematically in Fig. 1. The n^+ region is 0.35 μm long and its doping is 10^{17} cm^{-3}. The n region is 0.35 μm long and its doping is 10^{16} cm^{-3}. At the right side it is the Schottky barrier with the metal contact acting as a perfect absorbing boundary, that is, all the carriers reaching the metal leave the structure and no carrier is injected from the metal into the semiconductor. Since the depletion layer appearing near the Schottky contact changes with the biasing, the model must account for the variation of the number of particles inside the device according to the applied voltage. To this end an ohmic contact is simulated at the left side of the n^+ region. Charge neutrality is ensured at each time step in the cell closest to the ohmic contact by injecting carriers with the appropriate thermal distribution (velocity-weighted hemi-Maxwellian) at the lattice temperature T.[23] In this way the proper carrier dynamics inside the structure adjusts the number of electrons present in the diode at each time step according to the potential distribution, without any further artificial algorithm.[22] The barrier height considered in the simulation is 0.735 V, which leads to an effective built-in voltage at equilibrium V_{bi} of 0.640 V between the n region of the semiconductor and the metal. In our rather ideal model, we have not considered other phenomena which may also be present in real SBDs, such as: tunneling, image-force lowering of the barrier, quantum reflection, presence of defects at the semiconductor-metal interface, etc. Indeed, our primary objective is to provide a detailed analysis of an ideal diode, thus reaching a deep understanding of the processes responsible for the fluctuations, which are likely to be distorted with the inclusion of some of the effects previously mentioned. Moreover, the frequency range in which we are going to analyze the noise behavior of the SBD is well beyond the influence of $1/f$ contributions.

The calculations are performed by using an ensemble MC simulator (one-dimensional in real space and three-dimensional in momentum space) self-consistently coupled with a one-dimensional PS. The GaAs conduction band consists of three nonparabolic spherical valleys (Γ, L and X). The material parameters and the scattering mechanisms are the same as in Ref. 24. The MC simulation follows the standard scheme.[25] The device is divided into equal cells of 100 Å each, and the electric field is updated periodically at each time step (2.5 or 10 fs depending on the type of calculation) by employing the one-dimensional PS. The cross-sectional area adopted for the device in the simulation is 2×10^{-9} cm^2, which means an average number of simulated carriers around 7600 depending on the biasing. The simulation is performed at $T=300$ K.

III. NOISE CALCULATION: OPERATION MODES

In a one-dimensional uniform structure of length L with a single type of carriers (electrons), the total current flowing through any cross-section, $I(t)$, is given by:[26]

$$I(t)=I_c(t)-\frac{\varepsilon_0\varepsilon_r A}{L}\frac{d}{dt}\Delta V(L,t), \tag{1}$$

where ε_0 is the free space permittivity, ε_r the relative static dielectric constant of the material, A the cross-sectional area, $\Delta V(L,t)$ the instantaneous voltage drop between the terminals, and $I_c(t)$ the conduction current defined by $I_c(t) = -(q/L)\Sigma_{i=1}^{N_T(t)} v_i(t)$, with q the absolute value of the electron charge, $N_T(t)$ the total number of carriers inside the structure, and $v_i(t)$ the instantaneous velocity along the field direction of the ith particle.

Starting from Eq. (1), two alternative but complementary operation modes[26,27] are used to analyze the noise properties of the SBD:

(i) Current-noise operation, in which the applied voltage is kept constant in time and the current fluctuations are analyzed. In this case from Eq. (1) we obtain $I(t)=I_c(t)$. With this operation mode we investigate the effect of the coupling between fluctuations in carrier velocity and self-consistent electric field. To this end, under stationary conditions we will perform noise calculations with two different PS schemes. The first one is the *dynamic* PS, in which the time fluctuations of the self-consistent electric field are taken into account by solving the Poisson equation at each time step. In the second scheme we use a *static* PS so that the carriers move in the *frozen* nonfluctuating electric field profile. Of course, the PS scheme which is physically correct, is the dynamic one. The static case is just used to evaluate quantitatively the influence of the field fluctuations on the total noise.

(ii) Voltage-noise operation, in which the total current is kept constant in time and the voltage fluctuations are analyzed. By imposing the condition that the total current is constant in time, $I(t)=I_0$, from Eq. (1) we obtain:

$$\frac{d}{dt}\Delta V(L,t)=\frac{L}{\varepsilon_0\varepsilon_r A}[I_c(t)-I_0]. \tag{2}$$

By employing a finite-differences scheme, Eq. (2) allows one to calculate $\Delta V(L,t)$ in each time step during the simulation. Moreover, by solving the Poisson equation one can get $\Delta V(x,t)$ as a function of different positions x inside the device as measured from one of the terminals. With this operation mode we provide a spatial analysis of voltage noise by calculating the spectral density of voltage fluctuations as a function of position and frequency $S_V(x,f)$.[28]

In both modes the fluctuations are studied through the calculation of the respective current or voltage autocorrela-

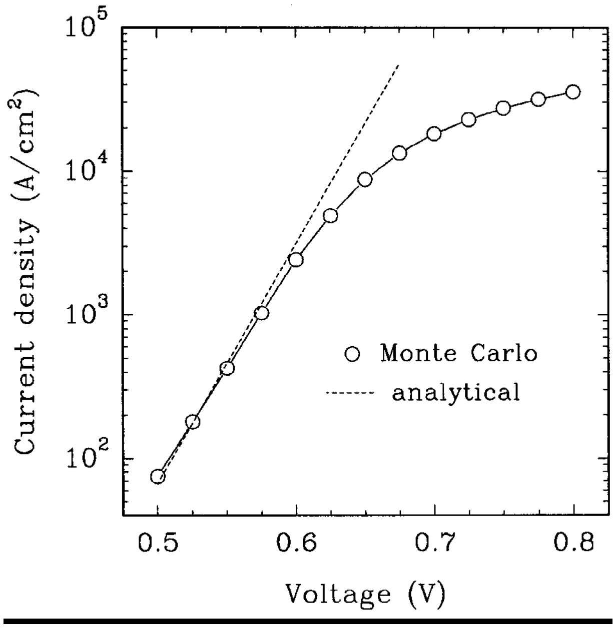

FIG. 2. Current-voltage characteristic of the Schottky barrier diode under forward-bias conditions. Circles (solid line) correspond to Monte Carlo calculations and dashed line to the analytical estimation according to thermionic emission theory.

tion functions $C_I(t)$ and $C_V(t)$ which, after being Fourier transformed, provide the spectral densities $S_I(f)$ and $S_V(f)$.[19] Once the stationary situation is reached in the simulation, the value of the current [voltage] $I(t)$ [$V(t)$] is recorded at each time step, for subsequent calculations of the corresponding autocorrelation functions. The simulation must be long enough to achieve a good time resolution of the autocorrelation functions. To this end, after a transient of 20 ps, the carrier kinetics is simulated for 0.75 ns in the case of current noise (time steps of 10 fs) and for 2.0 ns for voltage noise (time steps of 2.5 fs).

The equivalent noise temperature $T_N(f)$ (experimentally measurable) is a very important parameter for the characterization of the noise properties of SBDs. In our case we calculate its low-frequency value $T_N(0)$ from

$$T_N(0)=\frac{S_I(0)}{4K_B G(0)}, \tag{3}$$

when current-noise operation is employed [here $S_I(0)$ is the low-frequency value of the current spectral density, K_B the Boltzmann constant, and $G(0)$ the low-frequency differential conductance] and from

$$T_N(0)=\frac{S_V(0)}{4K_B R(0)}, \tag{4}$$

when voltage-noise operation is employed [here $S_V(0)$ is the low-frequency value of the voltage spectral density and $R(0)$ the low-frequency differential resistance]. Both $G(0)$ and $R(0)$ are obtained from the slope of the current-voltage (I–V) characteristics.[26]

IV. RESULTS

A. Static characteristics

Figure 2 shows the I-V characteristic of the SBD of Fig. 1. Only forward biasings higher than 0.5 V, which correspond to a semiconductor-metal barrier lower than $5K_BT/q$, have been simulated due to the limited statistical information that can be obtained with the number of particles used.[12] To simulate lower voltages (higher barrier) a particle-weighting scheme (with multiplication/compression of particles) would be necessary.[13] However, while appropriate to analyze the static characteristic of the devices, such an algorithm leads to the wrong results when dealing with noise calculations due to the different statistical weight of the carriers and fields producing the fluctuations. In agreement with expectations, two different regions can be clearly observed in the I-V characteristic according to the conditions $V<V_{bi}$ and $V>V_{bi}$. In the former, the current exhibits an exponential behavior which is determined by the thermionic emission of carriers over the metal-semiconductor barrier. In the latter, the current tends to assume a linear behavior due to the disappearance of the barrier, and the semiconductor series resistance controls the current in the diode. The dashed line in Fig. 2 shows the results for the current under forward-bias conditions given by the analytical thermionic emission theory:

$$J=\frac{qm^*(K_BT)^2}{2\pi^2\hbar^3}e^{-[q(\phi_m-\chi_s)/K_BT]}e^{(qV/K_BT)}, \tag{5}$$

where m^* is the effective mass of the electrons, $\hbar$ the reduced Planck constant, ϕ_m the work function of the metal, and χ_s the electron affinity of the semiconductor. $\phi_m-\chi_s$ corresponds to the barrier height, 0.735 V in our case. The agreement with the first region of the I-V curve is rather satisfactory and confirms the reliability of the MC simulations.

Figure 3 shows the stationary profile along the structure of several quantities of physical interest. While the semiconductor-metal barrier persists ($V=0.5$ V), the carriers remain thermalized [Fig. 3(c)] and a depletion region is observed near the Schottky contact [Fig. 3(a)] where all the potential drop takes place [Fig. 3(d)]. Beyond flatband conditions ($V=0.85$, 1.00 V) this depletion region practically disappears, leading to a more uniform potential gradient mainly located in the n region according to its higher resistance. This leads to the appearance of a relevant electric field which is responsible for a carrier heating along this region and subsequent intervalley transfer to higher L and X valleys. The velocity shows the expected behavior due to the presence of the barrier [Fig. 3(b)]. Since the Schottky contact acts as a perfect absorbing boundary and the movement of the electrons in the depletion region is practically ballistic, near the metal most of the carriers have positive velocities. For $V<V_{bi}$ the velocity distribution changes along the barrier from a full Maxwellian at the beginning of the barrier into a positive hemi-Maxwellian just at the boundary with the metal. This behavior, which is reported in Fig. 4, explains why the carrier velocity increases by approaching the metal contact, where it reaches a value of 2.1×10^7 cm/s. This value corresponds to $\sqrt{2K_BT/\pi m^*}$, the average veloc-

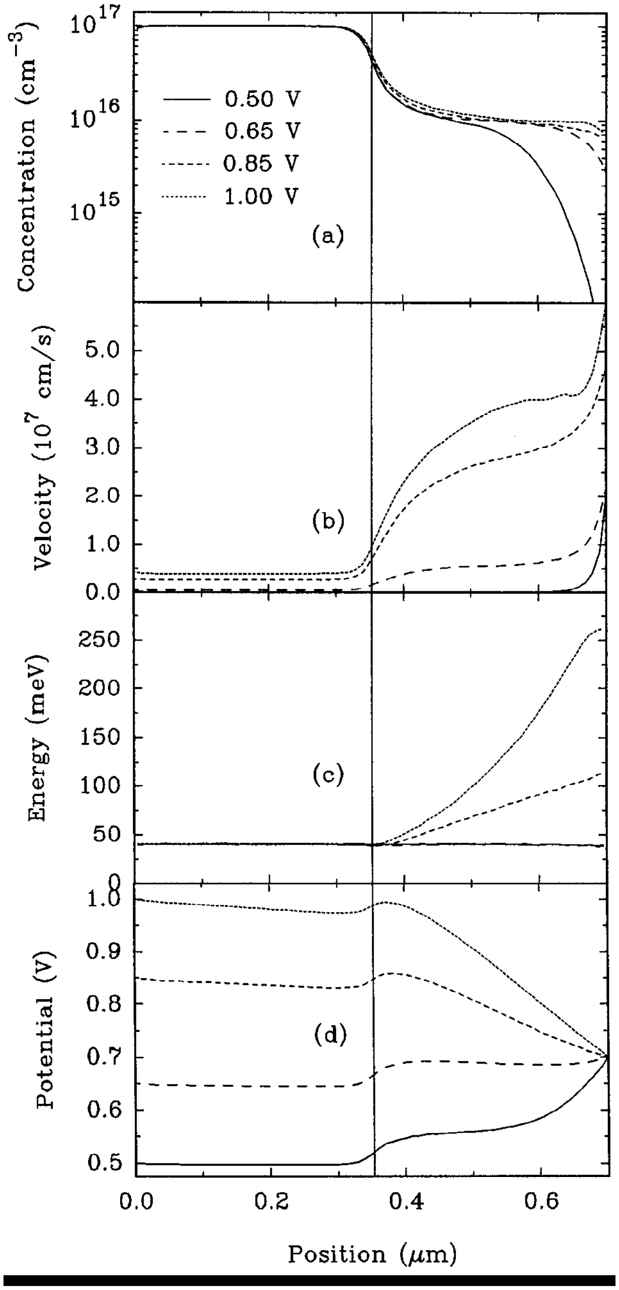

FIG. 3. Stationary profiles along the diode of different magnitudes: (a) free-carrier concentration, (b) average velocity, (c) average energy, and (d) potential for several applied voltages.

ity of a positive hemi-Maxwellian distribution, and sometimes is used as a boundary condition in the metal-semiconductor interface, despite some discrepancies about the correct value to be used.[9,11,12] In the case of $V > V_{bi}$, the presence of the electric field in the n region is superimposed on the previous effect, and therefore the velocity increases with the applied voltage. Moreover, due to the short length of the n region, overshoot velocities are observed, and values as high as 4.0×10^7 cm/s are reached.

A very important parameter in the ac behavior of the SBD is the junction capacitance. As we have already mentioned, the boundary conditions considered in the simulation allow for the variation of the number of carriers inside the structure with the applied voltage [Fig. 5(a)], from which the

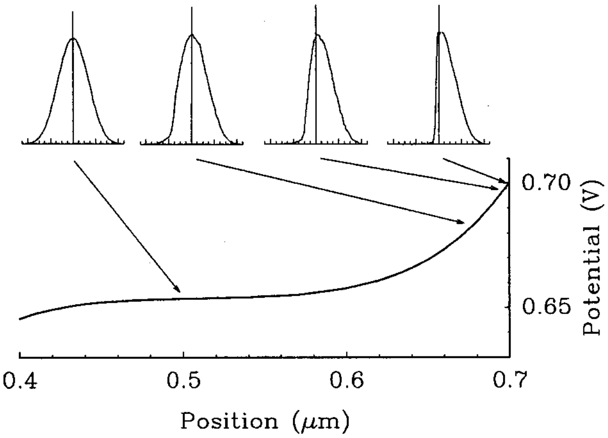

FIG. 4. Evolution of the carrier-velocity distribution along the n region of the diode for a biasing of 0.6 V. The distributions correspond to positions of 0.5000, 0.6750, 0.6950, and 0.6995 μm inside the diode. The potential profile of the n region is also shown.

capacitance of the diode can be calculated [Fig. 5(b)]. While the barrier persists ($V < V_{bi}$), the capacitance increases with the voltage in close agreement with the total depletion approximation (dashed line):

$$C = \left(\frac{q \varepsilon_0 \varepsilon_r N_D}{2(V_{bi} - V)} \right)^{1/2}, \tag{6}$$

where $N_D = 10^{16}$ cm^{-3} is the doping of the n region. $C = 3.02\times10^{-8}(V_{bi} - V)^{-1/2}$ F/cm^2 in our case. In this range the most important charge variation takes place in the depletion region close to the barrier [Fig. 3(a)]. When the voltage increases over 0.6 V, the capacitance decreases and is mainly related with the variation of the number of carriers around the n^+-n homojunction.

B. Current noise

Figure 6 shows the spectral density of current fluctuations $S_I(f)$ for different applied voltages calculated by using the static and dynamic PS schemes. Both schemes provide the same static characteristics, however the noise spectra are quite different because the dynamic PS includes the coupling between velocity and self-consistent field fluctuations. Let us focus on the dynamic results. For 0.575 V a first peak about 600 GHz appears, which is attributed to carriers that do not have sufficient energy to surmount the barrier with the metal and thus come back to the neutral semiconductor (*returning carriers*), as was originally proposed in Ref. 16. This peak disappears for 0.650 and 0.850 V, since for these voltages the barrier also disappears. A second peak at about 2200 GHz is observed for all the three voltages and is found to be related to the plasma frequencies of the n and n^+ regions. Thus, this peak originates from the coupling between fluctuations in carrier velocity and in the self-consistent field induced by the n-n^+ homojunction.[29] Its magnitude and frequency depend on the characteristics (doping and length) of the n and n^+ regions.[30] When a static PS is used, this second peak is completely washed out, thus supporting our interpretation. Another important result is that at low frequencies the

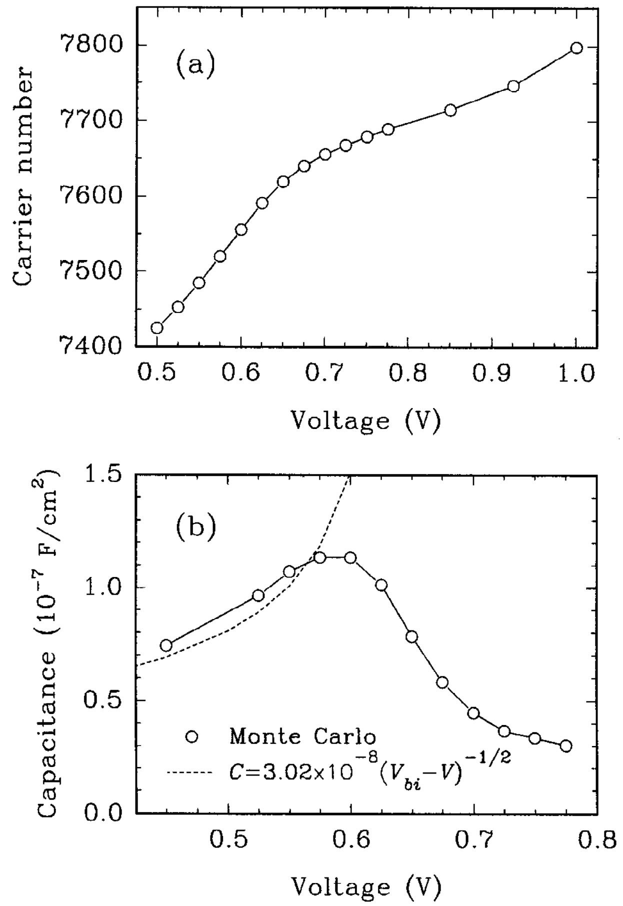

FIG. 5. (a) Number of carriers inside the Schottky diode and (b) associated capacitance as a function of the applied voltage. Circles (solid line) correspond to Monte Carlo calculations and dashed line to the analytical estimation according to the total depletion approximation.

values of $S_I(f)$ are significantly higher in the static scheme with respect to the dynamic one. In other words, the fluctuations of the self-consistent field strongly suppress the low frequency noise: a well known phenomenon in the case of vacuum tubes.[31]

In order to illustrate the effects associated with the returning carriers on the current-noise spectra, in Fig. 7 we present $S_I(f)$ and $S_I(f)-S_I(0)$ as a function of frequency in the range 10–1000 GHz for two voltages under which the semiconductor-metal barrier persists. In this frequency range we identify two contributions to the spectral density: a first one coming from carriers able to pass the barrier, which are responsible for $S_I(0)$ and whose contribution to $S_I(f)$ is constant with frequency;[16] and a second one originating from the returning carriers. As demonstrated in Refs. 16 and 32, the second group is responsible for a contribution which is proportional to f^2 until reaching a maximum whose amplitude and frequency are related to the height and width of the barrier. Figure 7 clearly shows how the f^2 dependence is detected in our results once $S_I(0)$ is subtracted from $S_I(f)$, thus confirming that the behavior of the spectra in this range is related to the returning carriers. The presence of the maximum is also detected, although somewhat masked by plasma effects which start appearing at these high frequencies.

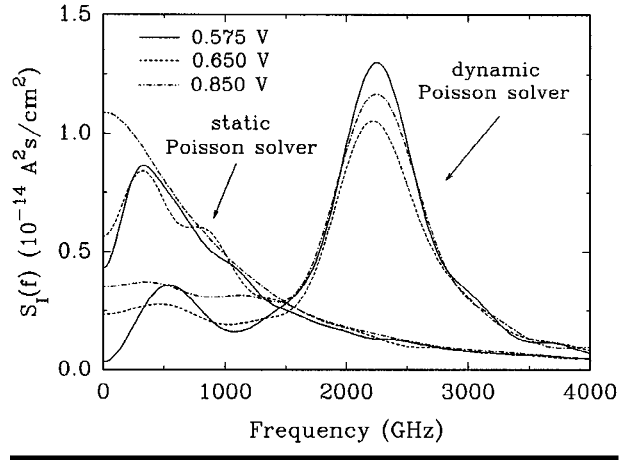

FIG. 6. Spectral density of current fluctuations as a function of frequency for several applied voltages, calculated by using a dynamic (instantaneous fluctuations of the self-consistent electric field are considered) and a static (neglected) Poisson solver.

Figure 8 presents the results for $S_I(0)$ as a function of the current, calculated by using static and dynamic PSs. Due to the spread in the time resolution of $C_I(t)$, the uncertainty of the calculations is estimated to be within 20%, a value comparable to the experimental counterpart. In the low-current region (corresponding to $V<V_{bi}$) $S_I(0)$ exhibits the $2qI$ dependence typical of a full shot-noise behavior caused by the carriers crossing the barrier individually and at random. When going to the high-current region the effect of the series resistance becomes increasingly important (since the built-in potential tends to disappear), and $S_I(0)$ deviates from the shot-noise behavior. In this region $S_I(0)$ approaches a value close to $4K_BT/R_S$, where T is the lattice temperature, corresponding to the thermal noise associated to the series resistance R_S (due to the n and n^+ regions in the device). This result is what is expected by assuming that carriers remain thermal with the lattice. Finally, for the highest currents, the appearance of an excess noise due to the onset of hot carriers and intervalley mechanisms is evidenced by a significant increase of $S_I(0)$.

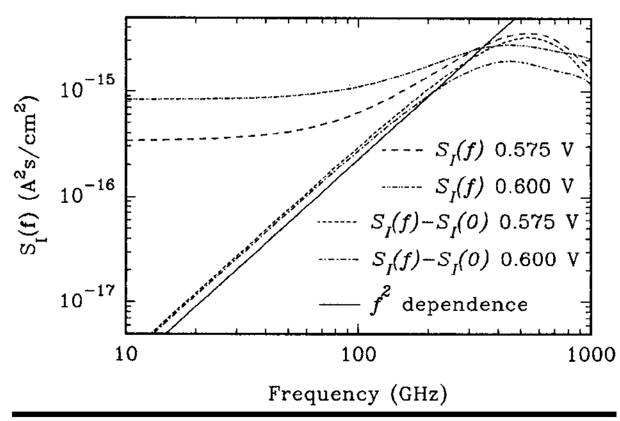

FIG. 7. Frequency dependence of the spectral density of current fluctuations (subtracting its low-frequency value) in the range 10–1000 GHz for biasings of 0.575 and 0.600 V. The dependence proportional to f^2 is also shown in the figure.

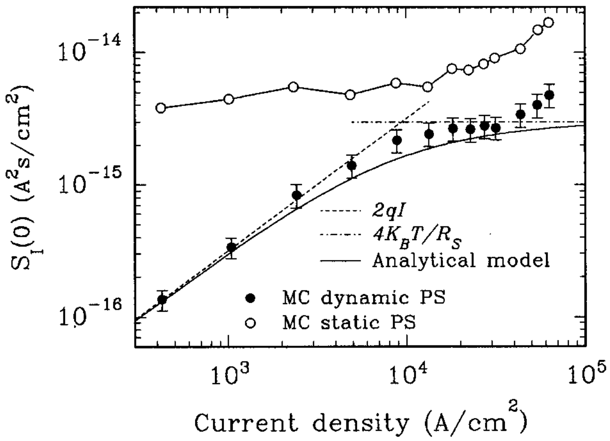

FIG. 8. Low-frequency value of the spectral density of current fluctuations as a function of the current calculated by using static and dynamic Poisson solvers, together with the analytical model of Ref. 16 and their asymptotic limits.

From a phenomenological point of view, $S_I(0)$ can be analytically expressed as the sum of a shot and thermal noise contribution from:[16]

$$S_I(0)=\frac{2qIR_j^2}{(R_S+R_j)^2}+\frac{4K_BTR_S}{(R_S+R_j)^2}, \tag{7}$$

where R_j is the junction differential resistance. Equation (7) predicts that for low currents, when $R_j \gg R_S$, the behavior of S_I is $2qI$, while for high currents, when $R_S \gg R_j$, it is $4K_BT/R_S$. The results of the dynamic simulation are favorably compared with this analytical model and its two limiting behaviors in Fig. 8. The value taken for R_j is obtained from the *I-V* characteristic in the exponential region, while that for R_S is calculated from the slope in the linear region, and it is about 5.5×10^{-6} Ω cm^2. The discrepancies between the MC results and the analytical model can be attributed to both the oversimplified model of Eq. (7) and the constant value assigned to the series resistance, whose determination is complicated due to the fact that it is expected to be voltage dependent.[15] Figure 8 also reports the values obtained for $S_I(0)$ with the static PS. While the *I-V* characteristics are the same, the results for $S_I(0)$ differ considerably with respect to the dynamic case, being systematically greater in the static case, where no transition from a shot-noise behavior to a thermal-noise behavior is observed. Indeed, at the lowest current $S_I(0)$ so calculated approaches the thermal value. Thus, the shot-noise behavior found with the dynamic PS turns out to be the result of a suppression of the thermal noise (detected in the static case) by means of the self-consistent field fluctuations. Such a suppression is a well known effect due to the presence of space charge.[31] In view of these results we emphasize the need to include a dynamic PS when studying noise spectra in SBDs, and more generally in nonhomogenous devices,[29,33] due to the essential role played by the coupling between fluctuations in carrier velocity and self-consistent electric field.

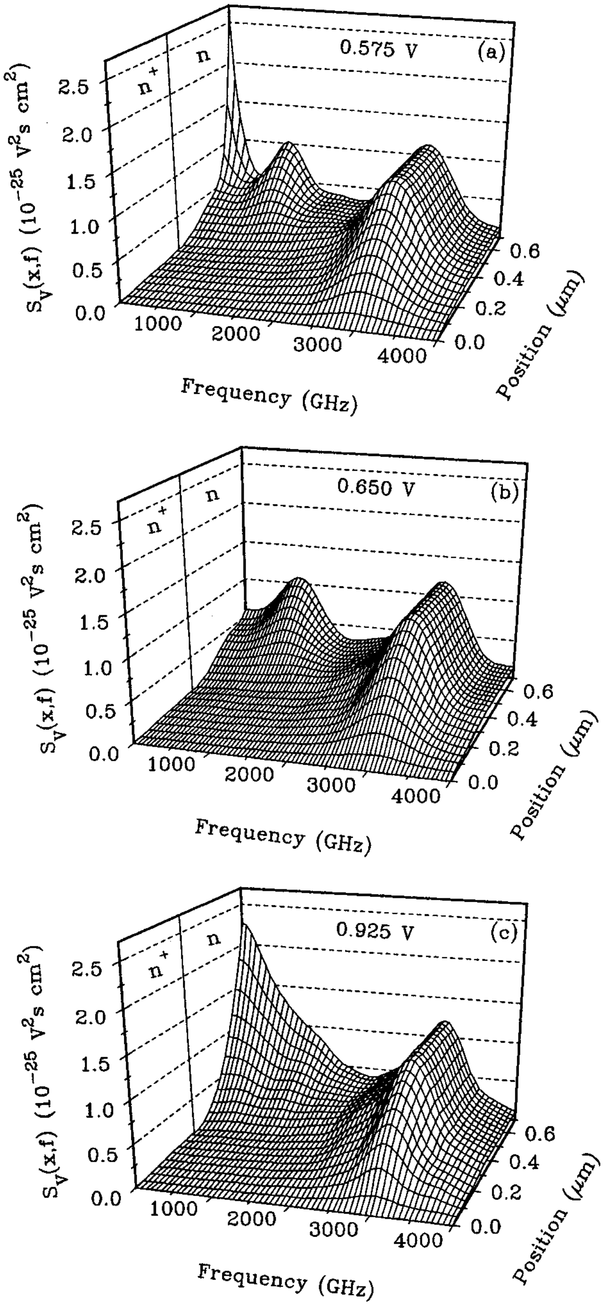

FIG. 9. Spectral density of voltage fluctuations as a function of frequency and position in the Schottky barrier diode for several average voltages: (a) 0.575 V (1.04×10^3 A/cm^2), (b) 0.650 V (8.82×10^3 A/cm^2), and (c) 0.925 V (5.41×10^8 A/cm^2).

C. Voltage noise

Figure 9 shows the result of a spatial analysis of the voltage spectral density in the SBD under study at three biasings for which the noise is controlled by different mechanisms. Here $S_V(x,t)$, calculated with respect to the ohmic contact, is shown as a function of position and frequency. The points $x=0$ μm and $x=0.7$ μm correspond to the positions of the ohmic and Schottky contact, respectively. In the high-frequency region, above about 1 THz, two peaks at the plasma frequencies of the n and n^+ regions of the structure are observed; each peak originates in the respective region. This is the well known effect of plasma oscillations

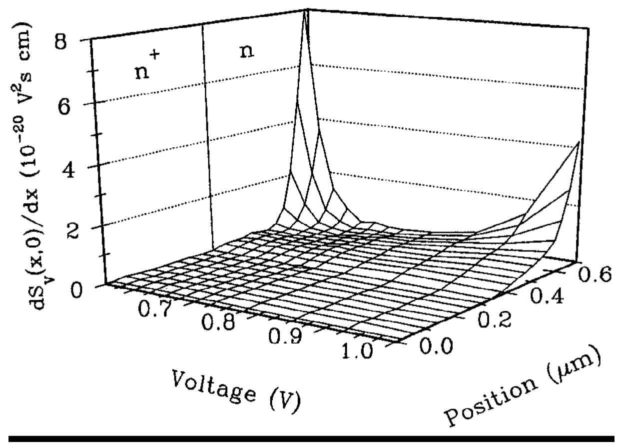

FIG. 10. Space derivative of the low-frequency value of the spectral density of voltage fluctuations as a function of position and mean voltage in the Schottky barrier diode under study.

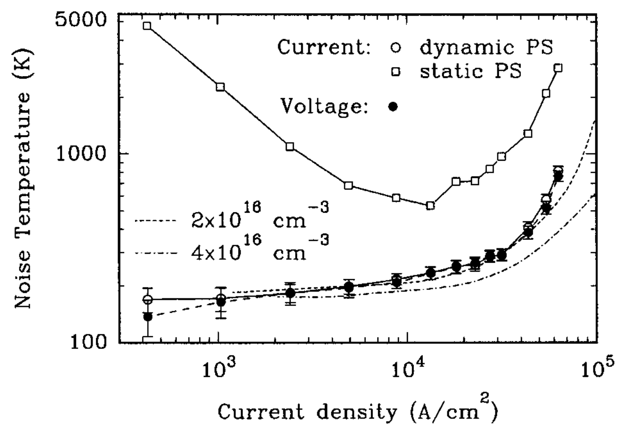

FIG. 11. Equivalent noise temperature at low frequency as a function of the current flowing through the diode. Circles correspond to Monte Carlo calculations performed considering a dynamic Poisson solver in the simulation and employing: current-noise operation (open circles) and voltage-noise operation (full circles). Squares correspond to calculations considering a static Poisson solver and making use of current-noise operation. The dotted and dash-dotted lines correspond to experimental data taken from Ref. 18, measured in Schottky barrier diodes with n layer doping of 2×10^{16} cm^{-3} and 4×10^{16} cm^{-3}, respectively.

already detected in other devices like n^+nn^+ structures.[19,28] At 0.925 V the great increase of the spectral density at low frequency practically washes out the peak related to the n region, while the high-frequency behavior above 2 THz remains practically the same.

On the contrary, the low-frequency behavior, which is related to the different mechanisms controlling the current throughout the device, changes significantly with the biasing. Figure 10 shows the space derivative of the low-frequency value of the voltage spectral density as a function of position and average voltage, $dS_V(x,0)/dx$. This magnitude is found to take significant values at different points inside the diode in going from the ohmic to the Schottky contact depending on the biasing, thus revealing the spatial origin of the voltage noise. For low voltages (in fact lower than the built-in potential at equilibrium, 0.640 V) shot noise is dominant, and most of the noise arises in the depletion region close to the barrier. At increasing voltages, when flatband conditions are reached, the noise becomes spatially more distributed. It mainly originates from the n region of the device and corresponds to the thermal noise associated with the series resistance. Finally, at the highest voltages, the presence of hot carriers and intervalley mechanisms in the n region is responsible for an excess noise contribution which leads $S_V(x,0)$ to increase significantly [see Fig. 9(c)]. In this last case there is no barrier, most of the voltage drop occurs in the n region of the device [see Fig. 3(d)] and the electrons become hot after traveling some distance under the action of the high electric field present in this region [see Fig. 3(c)]. For voltages higher than 0.775 V the electrons gain enough energy to transfer to the L valleys near the end of the n region. In these valleys the electrons have a larger effective mass, making this region highly resistive, and thus an important source of noise. This is the reason why $dS_V(x,0)/dx$ takes higher values and increases mainly near the Schottky contact. It is remarkable that this hot-carrier effect on the noise persists over a frequency range wider [see Fig. 9(c)] than that for which the noise is related to the depletion region near the barrier at the lowest voltages [see Fig. 9(a)].

D. Equivalent noise temperature

In Fig. 11 we show the equivalent noise temperature $T_N(0)$ at low frequency calculated from Eqs. (3) and (4) (i.e., under current- and voltage-noise operation modes, respectively) as a function of the current flowing through the diode, together with some experimental data taken from Ref. 18. Moreover, within current-noise operation, $T_N(0)$ has also been calculated with the static and dynamic PSs. For the case of the dynamic PS, the results obtained from both operation modes are found to practically coincide. At low currents, corresponding to the exponential region of the I-V characteristic, the noise temperature is close to half the value of the lattice temperature. This is a universal feature associated with the ideal forward I-V characteristic which reveals a full shot noise behavior, $S_I(0)=2qI$. As the current increases, the effect of the thermal noise in the series resistance becomes important and the noise temperature increases towards the lattice temperature, which is clearly crossed over for the highest currents because of the onset of the hot carrier effects described before. This behavior of $T_N(0)$ agrees favorably with that found by different experimental measurements,[15,17,18] as those shown in Fig. 11. Here the universal feature of the $T/2$ value at the lowest values of the current density is experimentally confirmed. On the other hand we have found a good qualitative agreement in the increase of $T_N(0)$ at higher current density, where a quantitative fitting would require the inclusion of the specific parameters of the measured diode in the simulation. In fact, for example, the simulated diode has an n layer doping of 10^{16} cm^{-3}, while in the case of the experimental data is of 2×10^{16} cm^{-3} and 4×10^{16} cm^{-3}. The higher the n layer doping, the higher the built-in voltage of the semiconductor-metal junction, and therefore the higher the current at which the noise temperature leaves the $T/2$ value and starts increasing. Concerning the results obtained with a static PS, while the I-V charac-

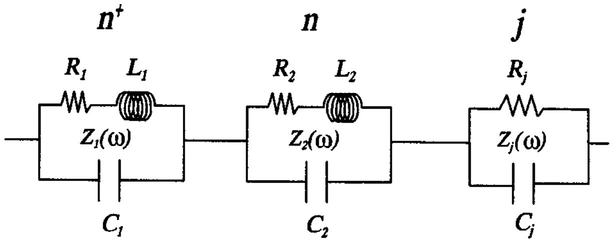

FIG. 12. Intrinsic small-signal equivalent circuit for the Schottky barrier diode at voltages lower than the built-in potential. Index 1 corresponds to the n^+ region, 2 to the neutral n region and j to the depletion region.

teristic was checked to remain the same, the values of $S_I(0)$, and thus of $T_N(0)$, differ considerably (being systematically higher) with respect to those obtained with a dynamic PS, as we have seen in Fig. 8. We remark on the essential role of the dynamic PS in determining the noise properties of these devices. This is especially clear for low currents, where the noise suppression due to the presence of the space charge near the barrier[31] is only detected when the dynamic PS is employed.

E. Small-signal equivalent circuit and noise spectra

To provide a quantitative interpretation of shot noise at low frequency and returning carriers and plasma effects at higher frequencies, in this section we propose a small-signal equivalent circuit for the SBD able to reproduce the whole current- and voltage-noise spectra when the current through the diode is controlled by thermionic emission ($V<V_{bi}$). Accordingly, the SBD can be represented by the series connection of three equivalent circuits representing each region of the device (n^+ region, neutral n region and j depletion region) as shown in Fig. 12.

The n^+ region and the neutral n region are represented by intrinsic equivalent circuits corresponding to homogeneous samples in which transport is controlled by collisions.[34] Here $R=l/(qN_D\mu)$ indicates the ohmic resistance of the sample (with μ the mobility, N_D the doping and l the length), $C=\varepsilon_0\varepsilon_r/l$ the capacitance of a parallel-plate capacitor whose dielectric is the sample and $L=m^*l/(q^2N_D)$ the inductance. These passive elements are related to the characteristic times of each region as: $L/R=\tau_m=m^*\mu/q$, $LC=\tau_p^2=\tau_m\tau_d=m^*\varepsilon_0\varepsilon_r/(q^2N_D)$ and $CR=\tau_d=\varepsilon_0\varepsilon_r/(qN_D\mu)$, where τ_m, τ_p and τ_d are the momentum, plasma and dielectric relaxation times of the material, respectively.[30] In this way the impedance corresponding to any of these two regions is:

$$Z(\omega)=R\frac{1+i\omega L/R}{1-\omega^2LC+i\omega CR}=R\frac{1+i\omega\tau_m}{1-\omega^2\tau_p^2+i\omega\tau_d}$$
$$=R\frac{1+i\left[\omega\tau_m(1-\omega^2\tau_p^2)-\omega\tau_d\right]}{(1-\omega^2\tau_p^2)^2+\omega^2\tau_d^2}. \tag{8}$$

$Z_1(\omega)$, corresponding to the n^+ region, is independent of the biasing, which is not the case of $Z_2(\omega)$, corresponding to the n region. In order to apply Eq. (8) to the neutral n region we must know its length l_2, which corresponds to 0.35 μm (n region length) minus the length of the depletion region (which depends on biasing). This last can be obtained from the stationary carrier concentration profile [see Fig. 3(a)], and it can also be estimated from the total depletion approximation. The mobility of the n and n^+ regions can be obtained from bulk MC simulations.

The junction (depletion region) is represented in the equivalent circuit by the standard parallel of its resistance R_j and its capacitance C_j, so that

$$Z_j(\omega)=\frac{R_j}{1+i\omega C_jR_j}=\frac{R_j(1-i\omega C_jR_j)}{1+\omega^2C_j^2R_j^2}. \tag{9}$$

Both R_j and C_j depend on the biasing. R_j is obtained by subtracting R_1+R_2 from the differential resistance obtained from the I-V curve, and C_j takes the values shown in Fig. 5(b).

The small-signal equivalent circuit of Fig. 12 can be applied to predict and explain the noise behavior of the diode in the whole frequency range for $V<V_{bi}$. Since under this condition both the n^+ and neutral n regions show an ohmic behavior and are practically at thermal equilibrium, the lattice temperature T is used to represent the noise related to them. In the case of the depletion region, since it is responsible for the appearance of shot noise, it will contribute to the noise with a temperature $T/2$. In this way, by using the Nyquist relationship, the voltage noise can be evaluated as:

$$S_V(\omega)=4K_BT\left\{\Re[Z_1(\omega)+Z_2(\omega)]+\tfrac{1}{2}\Re[Z_j(\omega)]\right\} \tag{10}$$

from which the current noise is obtained as $S_I(\omega)=S_V(\omega)/|Z(\omega)|^2$, where $Z(\omega)=Z_1(\omega)+Z_2(\omega)+Z_j(\omega)$ is the total impedance of the diode.

Figure 13 shows the comparison between the current- and voltage-noise spectra obtained with the equivalent circuit and from the MC simulation for an applied voltage of 0.575 V. The parameters of the equivalent circuit for this biasing take the values l_2 =0.20 μm, R_j =2.59$\times10^{-5}$ Ω cm^2 and C_j =1.13$\times10^{-7}$ F/cm^2. A reasonable agreement between both results is found. The equivalent circuit reproduces correctly the low-frequency values and the main features (frequency dependence, position of the maxima, etc.) of the noise spectra. Moreover, it is possible to associate the different effects detected in the spectra with the elements of the equivalent circuit and check in such a way the physical interpretation given to the MC results. Thus, the presence of the peak at 2200 GHz in $S_I(f)$ is related to the combination of $Z_1(\omega)$ and $Z_2(\omega)$ with their associated resonant plasma frequencies,[30] which is consistent with the physical explanation obtained from the simulation. Furthermore, the effect of the returning carriers leading to the initial f^2 behavior and the peak at 600 GHz is related to the presence of the capacitance C_j in $Z_j(\omega)$. In the case of $S_V(f)$ the two peaks at high frequency are associated, as expected, with the resonant plasma frequencies of $Z_1(\omega)$ and $Z_2(\omega)$, and the initial decrease of the spectrum with the effect of C_j. Of course both low-frequency values $S_I(0)$ and $S_V(0)$ are determined by the dominant role played by $Z_j(\omega)$ at low frequency.

The discrepancies found between the equivalent circuit and the MC results, especially important in the amplitude of

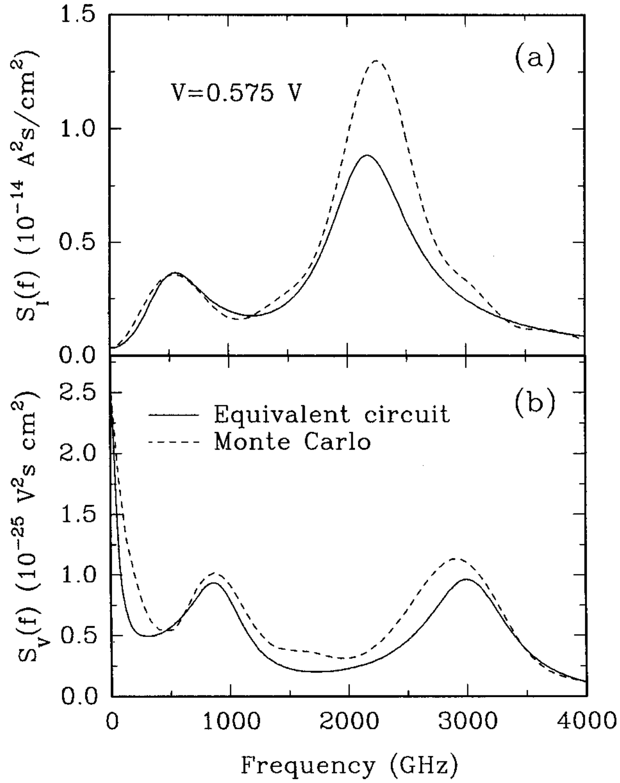

FIG. 13. Spectral density of (a) current and (b) voltage fluctuations for a biasing of 0.575 V (1.04×10^3 A/cm^2) obtained from Monte Carlo calculations (dashed lines) and from the equivalent circuit (solid lines).

the second maximum of $S_I(f)$, can be attributed to the fact that the circuit model neglects the free-carrier diffusion around the homojunction. To check this conjecture we have also simulated a GaAs SBD where this homojunction is suppressed. It consists of just a semiconductor n region of 0.4 μm with a doping of 5×10^{16} cm^{-3} surrounded by ohmic and Schottky contacts. In this case the equivalent circuit consists of just the series of $Z_2(\omega)$ (neutral n region) with $Z_j(\omega)$ (depletion region). Figure 14 shows the results obtained for $S_I(f)$ in this diode for two biasings. In this case, in the absence of the n^+-n homojunction, only the peak related to the returning carriers is observed. The frequency at which this peak appears is higher than in the previous case, since the doping of the semiconductor is higher and therefore the depletion region is shorter and the characteristic returning time is also shorter.[16] The agreement found between the equivalent circuit and the MC results is excellent. In particular, the low-frequency value and the amplitude and frequency of the maximum are nicely reproduced.

V. CONCLUSIONS

An ensemble MC simulator self-consistently coupled with a one-dimensional PS has been used to investigate the high-frequency noise properties of GaAs SBDs. This method, by intrinsically incorporating the processes causing the fluctuations, allows for a deep microscopic interpretation of the noise behavior of these devices. The main conclusions are the following:

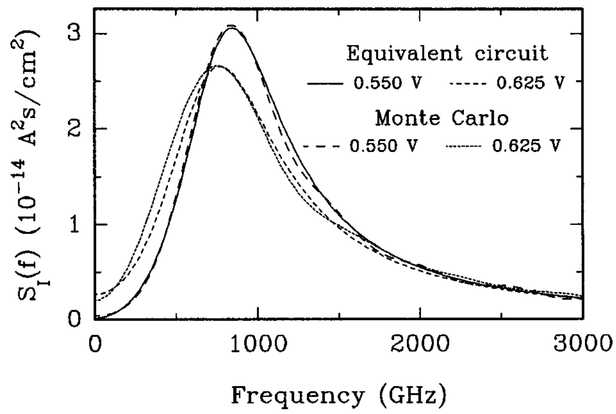

FIG. 14. Spectral density of current fluctuations for an homogenous GaAs Schottky barrier diode with length of 0.4 μm and doping of 5×10^{16} cm^{-3} for biasings of 0.550 and 0.625 V obtained from Monte Carlo calculations and from the equivalent circuit.

(i) The static characteristics of the diode are favorably compared with the existing theories on the ideal behavior of SBDs. Thermionic emission, series resistance and hot carrier regimes are detected.

(ii) By using current-noise operation, our microscopic model naturally detects the presence of shot, thermal and excess noise and reproduces their main features without invoking phenomenological noise sources. By employing static and dynamic schemes to solve the Poisson equation, the coupling between fluctuations in carrier velocity and the self-consistent field has been proven to essentially modify the noise spectra. In particular, it is responsible for the appearance of shot noise in the SBD by suppressing the thermal noise.

(iii) By using voltage-noise operation a spatial analysis of voltage noise has been performed, providing local information on the strength of the noise sources.

(iv) The results obtained for the equivalent noise temperature at low frequency show a behavior which is in agreement with experimental results. Theoretical predictions in the frequency region above 10 GHz need to be confirmed experimentally.

(v) A small-signal equivalent circuit able to reproduce the noise spectra under the thermionic emission regime has been proposed. The different features of the spectra are interpreted in terms of the elements of the equivalent circuit.

ACKNOWLEDGMENTS

Partial support from the NATO networking linkage Grant No. HTECH.LG 960931, from the Consejería de Cultura de la Junta de Castilla y León through Project No. SA11/96 and from the Comisión Interministerial de Ciencia y Tecnología through Project No. TIC95-0652 is gratefully acknowledged.

[1] N. R. Erickson, Proc. IEEE **80**, 1721 (1992).
[2] T. W. Crowe, R. J. Mattauch, H. P. Röser, W. L. Bishop, W. C. B. Peatman, and S. Liu, Proc. IEEE **80**, 1827 (1992).
[3] C. R. Crowell and S. M. Sze, Solid-State Electron. **9**, 1035 (1966).
[4] C. T. Chuang, Solid-State Electron. **27**, 299 (1984).

[5] J. Racko, D. Donoval, M. Barus, V. Nagl, and A. Grmanova, Solid-State Electron. **35**, 913 (1992).
[6] P. Van Mieghem, IEEE Trans. Electron Devices **ED-41**, 2440 (1994).
[7] S. F. Guo, Solid-State Electron. **27**, 537 (1984).
[8] U. Ravaioli, P. Lugli, M. A. Osman, and D. K. Ferry, IEEE Trans. Electron Devices **ED-32**, 2097 (1985).
[9] J. Adams and T.-W. Tang, IEEE Electron Device Lett. **EDL-7**, 525 (1986).
[10] U. V. Bhapkar and R. J. Mattauch, IEEE Trans. Electron Devices **ED-40**, 1038 (1993).
[11] G. Baccarani and A. M. Mazzone, Electron. Lett. **12**, 59 (1976).
[12] C. M. Maziar and M. S. Lundstrom, Electron. Lett. **23**, 61 (1987).
[13] M. J. Martín, T. González, D. Pardo, and J. E. Velázquez, Semicond. Sci. Technol. **11**, 380 (1996).
[14] T. J. Viola and R. J. Mattauch, J. Appl. Phys. **44**, 2805 (1973).
[15] E. L. Kollberg, H. Zirath, and A. Jelenski, IEEE Trans. Microwave Theory Tech. **MTT-34**, 913 (1986).
[16] M. Trippe, G. Bosman, and A. van der Ziel, IEEE Trans. Microwave Theory Tech. **MTT-34**, 1183 (1986).
[17] A. Jelenski, E. L. Kollberg, and H. Zirath, IEEE Trans. Microwave Theory Tech. **MTT-34**, 1193 (1986).
[18] S. Palczewski, A. Jelenski, A. Grüb, and H. L. Hartnagel, IEEE Microwave Guid. Wave Lett. **2**, 442 (1992)..
[19] L. Varani, L. Reggiani, T. Kuhn, T. González, and D. Pardo, IEEE Trans. Electron Devices **ED-41**, 1916 (1994).
[20] T. González, D. Pardo, L. Varani, and L. Reggiani, Appl. Phys. Lett. **63**, 3040 (1993).
[21] T. González, D. Pardo, L. Varani, and L. Reggiani, Semicond. Sci. Technol. **9**, 580 (1994).
[22] J. G. Adams, T.-W. Tang, and L. E. Kay, IEEE Trans. Electron Devices **ED-41**, 575 (1994).
[23] T. González and D. Pardo, Solid-State Electron. **39**, 555 (1996).
[24] T. Gonález, J. E. Velázquez, P. M. Guitérrez, and D. Pardo, Appl. Phys. Lett. **60**, 613 (1992).
[25] C. Jacoboni and P. Lugli, *The Monte Carlo Method for Semiconductor Device Simulation* (Springer, Berlin, 1989).
[26] J. Zimmermann and E. Constant, Solid-State Electron. **23**, 915 (1980).
[27] L. Reggiani, T. Kuhn, and L. Varani, Appl. Phys. A **54**, 411 (1992).
[28] T. González, D. Pardo, L. Varani, and L. Reggiani, Appl. Phys. Lett. **63**, 84 (1993).
[29] L. Varani, T. Kuhn, L. Reggiani, and Y. Perlés, Solid-State Electron. **36**, 251 (1993).
[30] L. Reggiani, P. Golinelli, E. Faucher, L. Varani, T. González, and D. Pardo, *Proceedings of the 13th International Conference on Noise in Physical Systems and 1/f Fluctuations*, edited by V. Bareikis and R. Katilius (World Scientific, Singapore, 1995), p. 163.
[31] A. van der Ziel, *Noise in Solid State Devices and Circuits* (Wiley, New York, 1986).
[32] A. van der Ziel, J. Appl. Phys. **47**, 2059 (1976).
[33] L. Varani, L. Reggiani, P. Houlet, J. C. Vaissiere, J. P. Nougier, and T. Kuhn, *Proceedings of Symposium on Fluctuations in Solids*, edited by J. Shikula (Technical University of Brno, Brno, 1992), p. 43.
[34] M. Shur, *GaAs Devices and Circuits* (Plenum, New York, 1987).